Topologically Protected Quantum Entanglement Emitters

Jianwei Wang (jianwei.wang@pku.edu.cn)
Peking University https://orcid.org/0000-0003-1313-9266

Tianxiang Dai
Peking University

Yutian Ao
Peking University

Jueming Bao
Peking University

Jun Mao
Peking University https://orcid.org/0000-0002-4043-2313

Yulin Chi
Peking University

Zhaorong Fu
Peking University

Yilong You
Peking University

Xiaojiong Chen
Peking University

Chonghao Zhai
Peking University

Bo Tang
Institute of Microelectronics, Chinese Academy of Sciences

Yan Yang
Institute of Microelectronics, Chinese Academy of Sciences https://orcid.org/0000-0002-0940-7013

Zhihua Li
Institute of Microelectronics, Chinese Academy of Sciences

Luqi Yuan
Shanghai Jiao Tong University https://orcid.org/0000-0001-9481-0247

Fei Gao
Zhejiang University https://orcid.org/0000-0001-9928-9390

Xiao Lin
Zhejiang University

Mark Thompson

University of Bristol https://orcid.org/0000-0002-2865-9558
Jeremy O'Brien
University of Western Australia
Yan Li
Peking University https://orcid.org/0000-0003-0607-3166
Xiaoyong Hu
Peking University
Qihuang Gong
Peking University

Article

Keywords: Reliable Quantum Applications, Silicon-photonic Chip, Einstein-Podolsky-Rosen Entanglement Emitters, Artificial Structure Defects

Posted Date: July 12th, 2021

DOI: https://doi.org/10.21203/rs.3.rs-640328/v1

Version of Record: A version of this preprint was published at Nature Photonics on February 17th, 2022.
See the published version at https://doi.org/10.1038/s41566-021-00944-2.

Topologically Protected Quantum Entanglement Emitters

Tianxiang Dai[1,10], Yutian Ao[1,10], Jueming Bao[1,10], Jun Mao[1,10], Yulin Chi[1,10], Zhaorong Fu[1], Yilong You[1], Xiaojiong Chen[1], Chonghao Zhai[1], Bo Tang[2], Yan Yang[2,⋆], Zhihua Li[2], Luqi Yuan[3], Fei Gao[4], Xiao Lin[4], Mark G. Thompson[5], Jeremy L. O'Brien[6], Yan Li[1,7,8,9], Xiaoyong Hu[1,7,8,9,⋆], Qihuang Gong[1,7,8,9,⋆], Jianwei Wang[1,7,8,9,⋆]

[1] *State Key Laboratory for Mesoscopic Physics, School of Physics, Peking University, Beijing, 100871, China*
[2] *Institute of Microelectronics, Chinese Academy of Sciences, Beijing 100029, China*
[3] *State Key Laboratory of Advanced Optical Communication Systems and Networks, School of Physics and Astronomy, Shanghai Jiao Tong University, Shanghai 200240, China.*
[4] *Interdisciplinary Center for Quantum Information, State Key Laboratory of Modern Optical Instrumentation, ZJU-Hangzhou Global Science and Technology Innovation Center, College of Information Science and Electronic Engineering, Zhejiang University, Hangzhou 310027, China*
[5] *Quantum Engineering Technology Labs, H. H. Wills Physics Laboratory and Department of Electrical and Electronic Engineering, University of Bristol, BS8 1FD, Bristol, United Kingdom*
[6] *Department of Physics, The University of Western Australia, Perth 6009, Australia*
[7] *Frontiers Science Center for Nano-optoelectronics & Collaborative Innovation Center of Quantum Matter, Peking University, Beijing, 100871, China*
[8] *Collaborative Innovation Center of Extreme Optics, Shanxi University, Taiyuan 030006, Shanxi, China*
[9] *Peking University Yangtze Delta Institute of Optoelectronics, Nantong 226010, Jiangsu, China.*
[10] *These authors contributed equally to this work. Emails to: yyang10@ime.ac.cn, xiaoyonghu@pku.edu.cn, qhgong@pku.edu.cn, jww@pku.edu.cn*

Entanglement and topology both portray nature at the fundamental level but in different manners. Entangled states of quantum particles are intrinsically sensitive to environment, whereas topological phases of matters represent natural robustness against environmental perturbations. Harnessing topology physics to protect entanglement thus has a great potential for reliable quantum applications. However, generating topologically-protected entanglement remains a significant challenge, which requires operating complex quantum devices in combined extreme conditions. Here we report topologically-protected quantum entanglement emitters, that emit topological Einstein-Podolsky-Rosen entangled state and topological multiphoton entangled state from a monolithically-integrated plug-and-play silicon-photonic chip in ambient conditions. The device emulating a photonic anomalous Floquet insulator allows the generation of up to four-photon topological entangled states at nontrivial edge modes. More importantly, we show that the Einstein-Podolsky-Rosen entanglement emitters can be topologically protected against artificial structure defects, by comparing tomographically measured fidelities of 0.968 ± 0.004 and 0.951 ± 0.01 for the perfect and defected emitters, respectively. Our topologically-protected entanglement emitters may find applications in photonic quantum computation and quantum simulation, and in the study of quantum topological physics.

Quantum mechanics has demonstrated that fundamental science can significantly drive profound applications. By harnessing quantum mechanical properties, it has eventually led to everyday semiconductor technologies, and continues to deliver significant improvements in information processing, measurement and security[1]. Entanglement[2] and topology[3] are two such featured quantum properties that describe nature at the fundamental level, and that offer significant opportunities to revolutionise information technologies. For example, quantum entanglement represents the counterintuitive nonlocal correlations between separated quantum particles[2]. Since the original proposal of the Einstein-Podolsky-Rosen (EPR) entangled state[4], entangled states with dozens of quantum particles have been demonstrated in various systems, e.g., photons[5], atoms[6], and superconducting[7] systems, for the implementations of classically intractable tasks of quantum computing[8,9] and quantum simulation[10]. Furthermore, topology represents the global invariant of wavefunctions on the entire band structure[3]. Since the first discovery of integer quantum Hall effect in condensed matter systems[11], topological phases have been observed in photons[12], atoms[13], and acoustic[14] systems, promising the development of topological devices immune to impurities and disorders. These fundamental differences of entangled states and topological phases make them behave in significantly different but potentially complementary manners. It is known that entangled states are fragile in respect of decoherence and fidelity degradation in noisy environment particularly in largely entangling systems[5–7]. Therefore, the adoption of topology nature has great potentials to immunize entanglement against imperfections. However, generating topologically-protected entanglement remains significantly challenging, particularly in electronic quantum devices, which requires complex quantum devices able to simultaneously interoperate the emergence of topological nontrivial phases in strong magnetic field[3,11] and the preparation of entangled states in millikelvin low temperature or high vacuum[6,7]. The emergent topological photonic systems provide an alternative possibility[12,15–23]. Significant progress in topological quantum photonics includes for examples the topological transport of pre-produced entangled states[24–26], quantum interference at topological beamsplitters[27,28], and the generation of topological single-photon and biphoton states[29–31]. The photon-number entangled states with biphoton have been generated in a Su-Schrieffer-Heeger topological device with deliberately introduced disorders[32]. However, topological EPR entanglement emitters that likely play as the keystone for topological quantum technologies, have not been directly realized experimentally, nor have their topological protection against certain defects and multiphoton topological entanglement been experimentally investigated. See an additional note in the end of the article.

In this work, we report experimental demonstrations of the emergence of topological Einstein-Podolsky-Rosen entanglement in complementary metal-oxide-semiconductor (CMOS) silicon chips in ambient conditions. The topological entanglement emitters monolithically integrate all optical components, and they are compact, phase stable, and plug-and-playable. Topological entangled states are produced at the nontrivial edge modes of an emulated anomalous Floquet insulator lattice, and verified by quantum interferometric and tomographical measurements, and demonstrations of Bell violation. For the first time (to the best of our knowledge), we experimentally demonstrate topologically-protected EPR entanglement emitters in the presence of artificially induced structure defects, and the generation of multiphoton (photon-number) topological entangled state. Our developed topological quantum devices possess both superiorities of integrated topological photonics[15–17], and integrated quantum photonics[33–36] that allows efficient photon generation[37], precise quantum operation[38], and large-scale quantum integration[39], potential to enhance photonic quantum information processing[40–42].

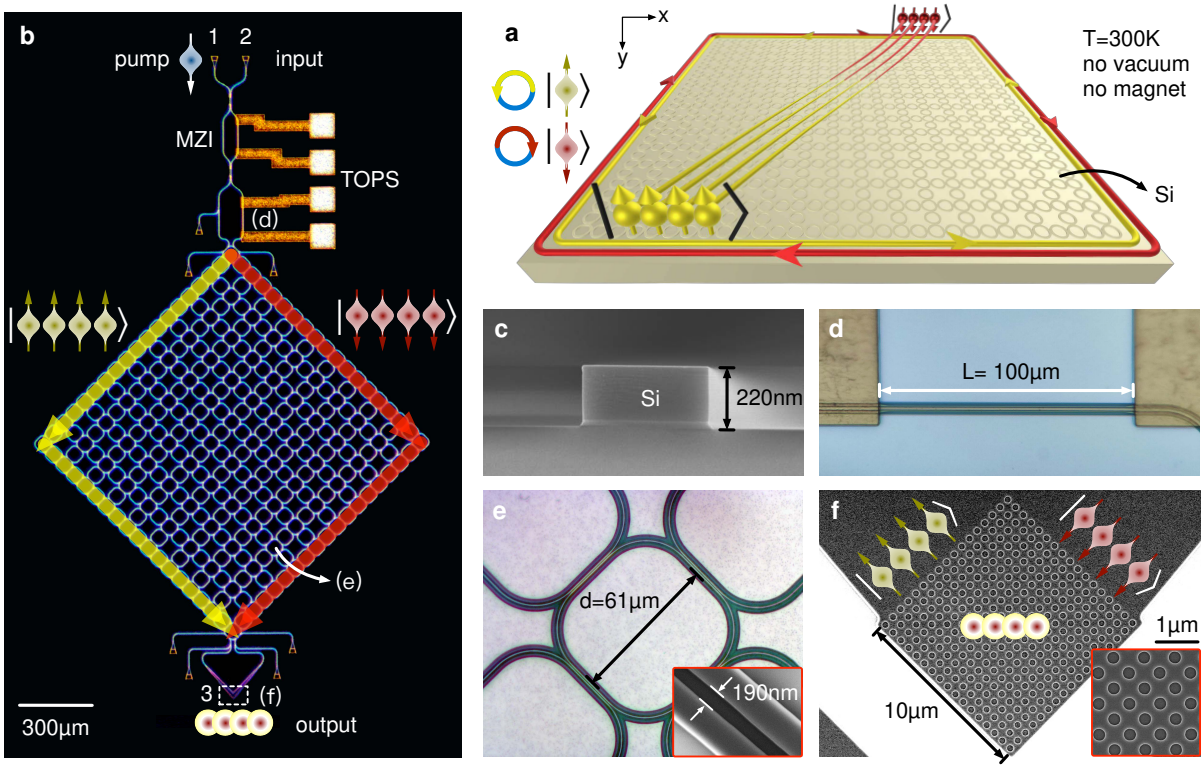

Figure 1 A topological quantum entanglement emitter in a photonic anomalous Floquet topological insulator. **a** and **b,** Diagram and optical microscope image of a topological quantum device, in which entangled photons emerge and flow at a pair of edge modes, while insulate and dissipate in the bulk lattice. Opposite pseudospin photons (pseudospin up $|\uparrow\rangle$ and down $|\downarrow\rangle$ states) occupy opposite propagation direction in the rings (CCW and CW modes), forming the logical basis of topological pseudospin qubits. The device emits topological entanglement in pseudospin single photons. The device is fabricated by silicon-photonics CMOS processes, and none of cryogenics, vacuum and magnet is required in the process of generating topological quantum entanglement. The device bases on a photonic anomalous Floquet topological insulator that consists of a 10×10 lattice of strongly coupled microring resonators, in total 280 identical microring. When the nontrivial edge modes emerge at the boundary of the lattice (indicated by the big yellow CCW and red CW arrows), it allows efficient generation of single photons by spontaneous FWM. Topological quantum states including fully separated states and maximally entangled states (*e.g.,* topological EPR state $(|\uparrow\uparrow\rangle + |\uparrow\uparrow\rangle)/\sqrt{2}$) can be generated by reconfiguring the excitation via an integrated Mach-Zehnder interferometer (MZI). Importantly, the topologically entangled states are intrinsically robust against certain fabrication disorders and induced structure defects. The device is terminated by a two-dimensional grating coupler (port 3) that ensures quantum coherent superposition of pseudospin up and down states, and diffracts photons into fee-space for state analysis. One-dimensional grating couplers are used for excitation injection (through ports 1, 2) and also tapped out for characterizations (those not labelled). **c–f,** Scanning electron microscope (SEM) and optical microscope images for photonic components: **c,** silicon nanowaveguide with a cross section of 450nm $\times$ 220nm, **d,** thermo-optical phase-shifter (TOPS) with a 2 μm-width and 100 μm-length resistive TiN layer, **e,** strongly coupled microring resonators with a diameter of 61 μm, inset: zoomed-in view of directional coupler with a gap of 190 nm and coupling length of 20 μm, and **f,** 70 nm shallow etching two-dimensional grating coupler consisting of a 605 nm periodic array of 390 nm-diameter holes.

Figure 1 illustrates the topological quantum entanglement emitter in the photonic anomalous Floquet topological insulator[43–50]. The device is made of silicon nanowaveguides (Fig.1c), and consists of a square lattice of 10 unit cells by 10 unit cells strongly coupled microring resonators (Fig.1e), in total 280 identical rings each with a diameter of 61 μm. Floquet nontrivial phases are formed in the absence of magnetic field by periodic evolution of light in the lattice, emulating a periodically driven Hamiltonian, which is fundamentally distinct to the type of integer quantum Hall insulator[19,20]. The ring lattice in Figs.1a,b can be described by a network model of $S(k)\,|\Psi\rangle = e^{i\psi}\,|\Psi\rangle$, where $S(k)$ is the transfer matrix of Bloch wave vector k, and $|\Psi\rangle$ is the wavefunction. The device exactly represents an anomalous Floquet insulator with a quasienergy of ψ/T, when $S(k)$ is regarded as a time-evolution operator over a period of T, *i.e.*, $S(k) = \mathcal{T}\exp[-i\int_0^T H_k(t)\,dt]$, where $\mathcal{T}$ is a time-ordering operator[43,44]. The topology of band structure is determined by a quantity of coupling strength (Θ) between site rings, which can be explicitly described by the coupling coefficiency of directional couplers (see inset in Fig.1e). When $\Theta > \pi/4$, the device is topologically nontrivial[43,51]. Details of network model and device fabrication are provided in Supplementary Information Sec.1 and Sec.2.

Figure 2a reports the calculated band structure in the first Brillouin zone for the entire microring lattice. In the band gap between bulk bands, both of which have a zero Chern number (C), two pseudospin topological edge states emerge, when considering the lattice as a stripe that is infinite along the x-axis but finite at the y-axis. The topological invariant can also be described by a winding number (W) for the band gaps ($W = 1$ when Θ exceeds $\pi/4$)[46,52]. The pseudospin up $|\uparrow\rangle$ state and pseudospin down $|\downarrow\rangle$ state are represented by counter-clockwise (CCW) and clockwise (CW) photon propagation directions in the site rings, respectively[43–46,51,53]. The excitations of $|\uparrow\rangle$ or $|\downarrow\rangle$ state, or their superposition state can be well controlled by a reconfigurable MZI prior to the lattice (see Fig.1d). Figures 2b,c show the measured transmission spectrum of the pseudospin up and down states, respectively, that are in good agreement with theoretical calculations. Fabrication disorders among the rings (*e.g.,* coupling strength, resonance conditions) are included in calculations (Sec.1). Both spectra within bulk-state windows for the pseudospin up and down modes are significantly random, whereas those within edge-state windows (*i.e.,* within gaps) are highly consistent and indentical. This suggests the topological robustness of nontrivial edge modes, but not for bulk modes, in the presence of inevitable fabrication disorders in nanodevices. Within one free-spectral range

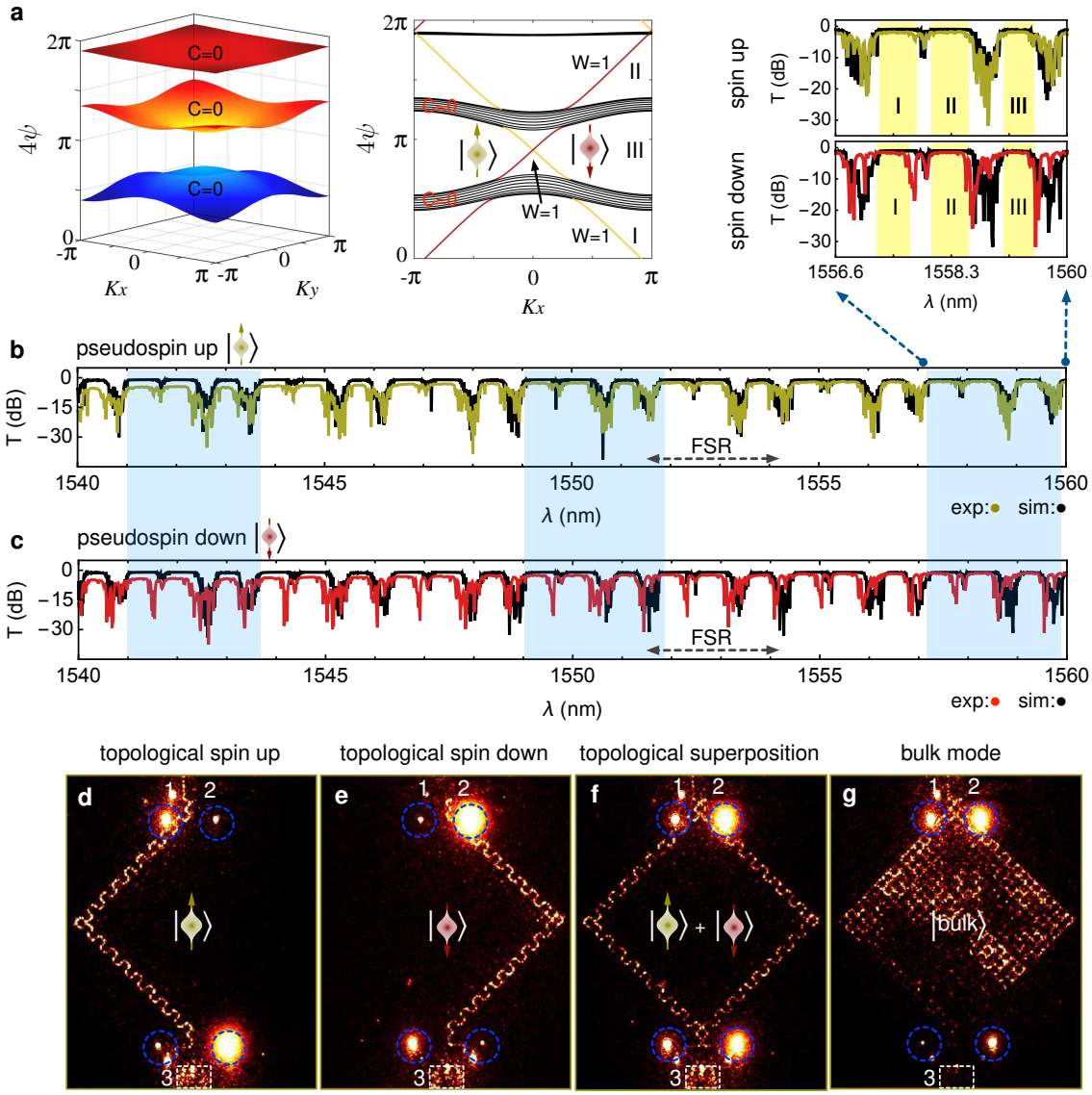

Figure 2 Characterizations of the topological quantum entanglement device. a, Calculated band structure for the photonic anomalous Floquet topological insulator. The 4ψ value is the propagation phase across a single site ring which represents the quasienergy of topological insulator. The Chern number (C) describes the topological invariant of band structures. The topology of band structure is determined by the coupling strength (Θ) between site rings. The projected band indicates the presence of two edge states, *i.e.*, pseudospin up (CCW) and pseudospin down (CW) edge states, when the device is topological nontrivial given $\Theta > \pi/4$. **b** and **c,** Transmission spectra for pseudospin up and down states. Yellow and red points are experimental results (measured by individually exciting the pseudospin state), and black points are simulation results (calculated by a network model for the 10×10 entire lattice). Inset shows spectra within one FSR. Three plateaus in one FSR (zones I, II, and III) confirm high transmission of photons along the topological edge modes, while dips of low transmittance indicate the dissipation of photons in the entire lattice as bulk states. Note that experimental results contain spectral response of grating couplers; simulation results contain phase disorders among rings due to fabrication disorders. We implemented experiments in blue-colored windows. **d–g,** Measured real-space distributions of electromagnetic fields in different modes: **d,** topological pseudospin up edge mode, **e,** topological pseudospin down edge mode, **f,** topological superposition of the two edge states, and **g,** bulk mode. Images were captured by an InGaAs infrared camera. For comparison, in Fig.S10, it shows the spectra and field distributions of two topological trivial devices. The port-3 (dashed white box) in (d–f) indicates the two-dimensional grating coupler that diffracts the topological edge states into free-space (note bright emission has been collected by an optical fiber to avoid strong camera saturations), while it implies dark emission for the bulk state (port-3 in (g)). Bright spots (in dashed blue circles) are visible because of out-of-plane light diffraction from one-dimensional grating couplers that are tapped out for device characterizations.

(FSR), we observed three wide plateaus of edge states, repeated for other FSRs (Sec.1). This feature of anomalous Floquet topological insulator thus allows the generation of broadband entangled photons.

Figures 2d-f report the measured field distributions of the pseudospin up $|\uparrow\rangle$ and pseudospin down $|\downarrow\rangle$ edge states, and a superposition of two pseudospin edge states $(|\uparrow\rangle + |\downarrow\rangle)/\sqrt{2}$. The excitation of these states are controlled by the MZI. Unambiguous topological transports of wavefunctions of invariant pseudospin edge states are observed along the boundary of the lattice. In contrast, Fig.2g shows the measured field distributions of bulk states in the Fig.1b device (see simulation in Fig.S2), in which energy is distributed into the entire lattice. Supplementary Movies S1-S3 show real-time measurement of field distributions of topological pseudospin states with a continuous scan of wavelength. Figure S10 shows the experimental results of a two-dimensional and one-dimensional topological trivial emitters, confirming their lacks of immunity to disorders.

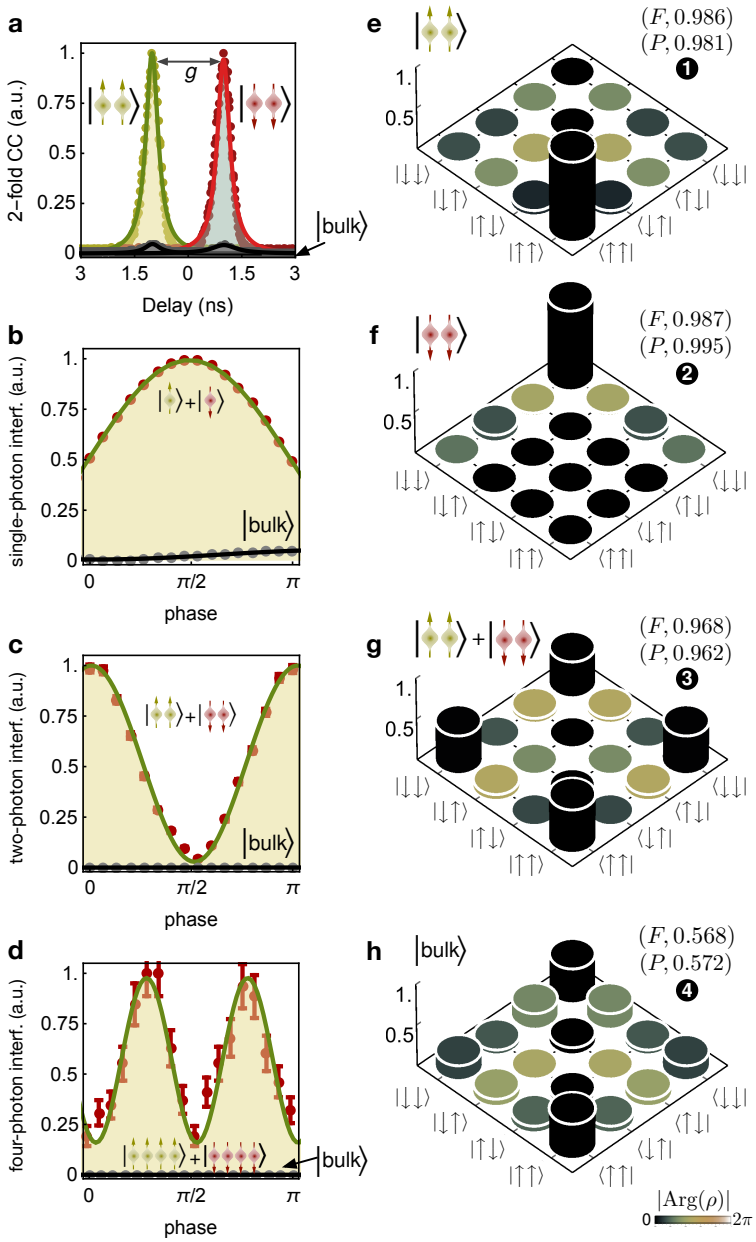

Figure 3 Experimental demonstrations of topological quantum entanglement. a, Measurement of two-fold photon coincidence counts (C.C.) in the topological quantum device in Fig.1b. Two pseudospin states $|\uparrow\uparrow\rangle$ and $|\downarrow\downarrow\rangle$ were generated in the edge modes (red and green colored data) and bulk modes (black data). A high contrast of 22:1 of C.C. was measured between the edge and bulk states. Such nonlinearity enhancement is owning to the concentration of topological edge modes along the lattice boundary where the pump, signal and idler photons strongly overlap and co-mode propagate, and also owning to its linear-dispersion band-structure (Fig.2a) that naturally meets the phase matching condition. These properties are however lacked in bulk modes. Note a shifted delay (g) is added in purpose for clarity. **b–d,** Measurement of classical interference and quantum interference in the topological edge modes (red data): **b,** single-photon ("λ") classical interference, V=0.993 ± 0.001, **c,** two-photon ("$\lambda/2$") quantum interference, V=0.933 ± 0.006, **d,** four-photon ("$\lambda/4$") quantum interference, V=0.724 ± 0.055. The V value refers to interference visibility, defined as $(N_{\max} - N_{\min})/(N_{\max} + N_{\min})$, where N is the measured photon counts. When the bulk-state was excited (black data), no apparent quantum interference and entanglement was observed. In (a–d), points are experimental data, and lines are fitting. Data for edge and bulk states were measured under the same experimental conditions; bulk-state results are normalised to edge-state results. **e–h,** Experimentally reconstructed density matrices for different topological quantum states, which are all generated in the Floquet quantum device: **e,** topological pseudospin up edge state $|\uparrow\uparrow\rangle$, F=0.986 ± 0.004, P=0.981 ± 0.008; **f,** topological pseudospin down edge state $|\downarrow\downarrow\rangle$, F=0.987 ± 0.003, P=0.995 ± 0.006; **g,** topological pseudospin EPR entangled state $(|\uparrow\uparrow\rangle + |\downarrow\downarrow\rangle)/\sqrt{2}$, F=0.968 ± 0.004, P=0.962 ± 0.008; and **h,** bulk state, F=0.568 ± 0.016, P=0.572 ± 0.016. An over-complete quantum state tomography technique with 36 measurements was implemented to reconstruct the density matrices. The F value denotes state fidelity that is defined as $\langle\phi_0|\rho|\phi_0\rangle$, and the P value denotes state purity that is defined as $\mathrm{Tr}[\rho^2]$, where ρ is the reconstructed state and $|\phi_0\rangle$ is the ideal state. Column heights represent the absolute values ($|\rho|$) of the elements of density matrices, and colors represent their phases $|\mathrm{Arg}(\rho)|$. For comparison, in Fig.S10, it shows experimental density matrices of two trivial quantum devices. Degenerated excitation was adopted for the measurement in (d), while non-degenerated excitation for all other measurements. Longer time of data collection was applied in (h). All error bars (one *s.d.*) are estimated from photon Poissonian statistics; those in (c) are smaller than data points.

Logical qubit states are represented by pseudospin information of single photons, *i.e.*, encoded in a superposition of pseudospin up $|\uparrow\rangle$ and pseudospin down $|\downarrow\rangle$ states as $\alpha|\uparrow\rangle + \beta|\downarrow\rangle$, where α, β are complex amplitudes, see Fig.1a. We adopt the intrinsically strong four-wave mixing (FWM) nonlinearity of silicon nanowaveguides to create topological pseudospin entangled photons. When excitation photons transport along the edge modes, pairs of signal and idler photons can be generated with a high efficiency, as a result of concentration of excitation fields at the boundary, linear-dispersion for phase matching (see right plot in Fig.2a), and co-mode propagation and strong interaction of the annihilation and creation fields at the edges. When excitation is in bulk modes, the dissipative nature (Fig.2g) and random transmission (Fig.2b,c) prevent single photon generation. We chose single-photons at the wavelength of 3-FSR away from the excitation. Figure 3a reports measured photon-pair coincidences, showing a 22 times enhancement of FWM between the edge and bulk modes. It suggests an efficient nonlinear-optical process at the topological edge modes. Strong spectral correlations of emerged photons in edge modes are confirmed, see results in Fig.S7.

The emitter allows the generation of a range of topological quantum states. For example, separated topological pseudospin up state $|\uparrow_s\uparrow_i\rangle$ (down state $|\downarrow_s\downarrow_i\rangle$) can be created by individually exciting the CCW (CW) edge mode, where subscripts refer to the signal and idler photons (we omit for clarity). Topological pseudospin entangled state of $(cos(\frac{\theta}{2})|\uparrow\uparrow\rangle + e^{i2\phi}sin(\frac{\theta}{2})|\downarrow\downarrow\rangle)$ can be generated by coherently and simultaneously exciting the two edge modes, where the phases of $\{\theta, \phi\}$ are on-chip manipulated. For $\theta = \pi/2$ it yields the maximally entangled topological EPR state or Bell state. It can also lead to topological multiphoton entangled states with high power excitation of the edge modes. We remark in our anomalous Floquet quantum device, the pseudospin up $|\uparrow\rangle$ and pseudospin down $|\downarrow\rangle$ qubit states in the edge modes are emerged at the same wavelength and own identical spectral distributions (Figs.2b,c) – this make it distinct to the photonic quantum Hall devices[19,20,30] in which the two edge modes emerge in different wavelength. This is key in our experiment, as it ensures high quantum indistinguishability of single photons produced in the two edge modes, and therefore leads to coherent topological superposition and topological entanglement of

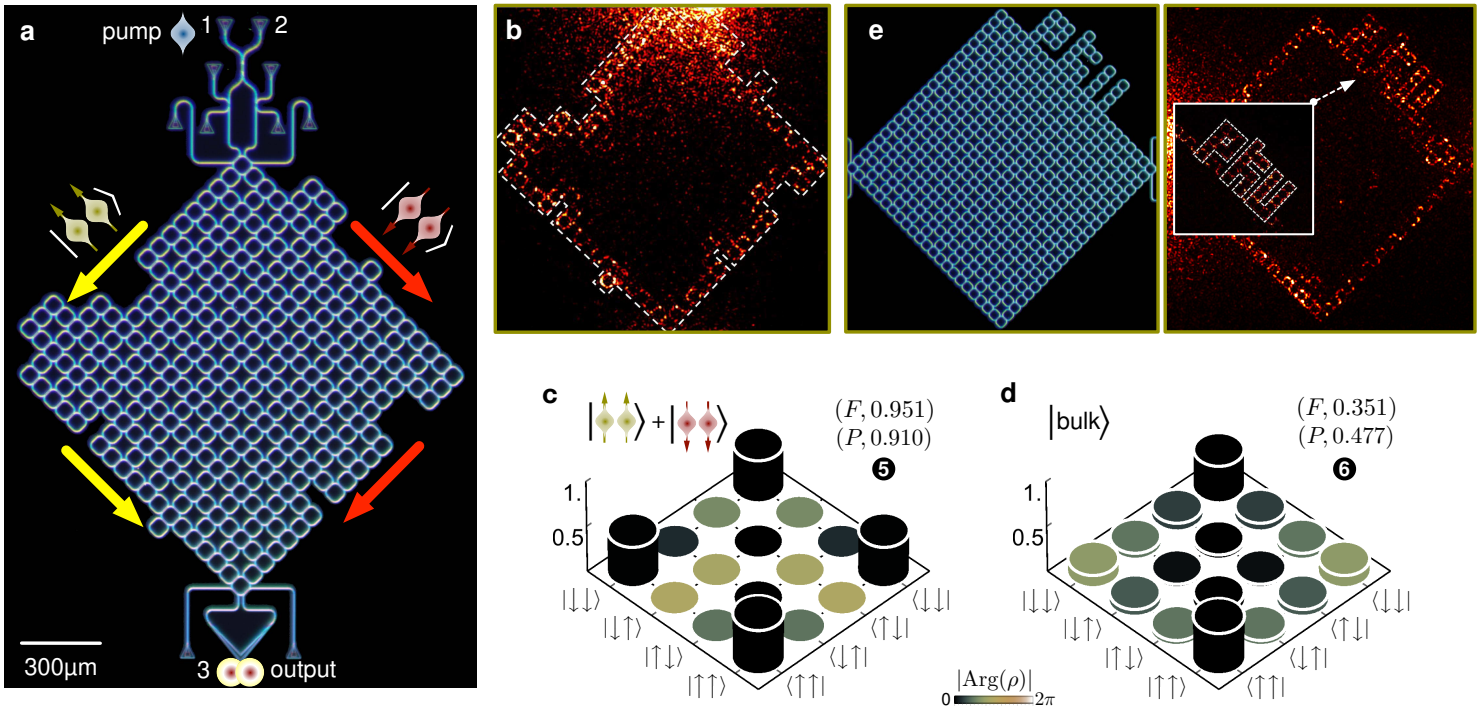

Figure 4 Topological protection of quantum entanglement against certain imperfections. An anomalous Floquet topological entanglement device containing four different types of artificial structure defects: **a,** optical microscope image of the device; **b,** measured field distribution of the pseudospin up and down topological nontrivial states along the CCW and CW edges (indicated by big yellow and red arrows) where artificial defects are embedded in. The Floquet microring lattice structure was designed by adding and removing a single link ring and a unit cell. See Fig.S3 for simulation results of field distributions. **c,** Experimentally reconstructed density matrix for the topological EPR entangled state $(|\uparrow\uparrow\rangle + |\downarrow\downarrow\rangle)/\sqrt{2}$ emerged in the imperfect quantum device in (a). The observations of high fidelity of 0.951 ± 0.010 and high purity of 0.910 ± 0.019 demonstrate the topological protection of entanglement, that is immune to structure defects. **d,** Reconstructed density matrix for the bulk state with F=0.351 $\pm$ 0.027 and P=0.477 $\pm$ 0.016. Over-complete quantum state tomography was implemented to reconstruct the density matrices. Column heights represent the absolute values ($|\rho|$) of the elements of density matrices, and colors represent their phases $|\mathrm{Arg}(\rho)|$. All error bars (± 1 *s.d.*) are estimated from photon Poissonian statistics. **e,** Another example of topological device embedded with the "PKU" arranged imperfections and its measured topological edge states. Dashed white lines in (b) and (e) are provided as a guide to the eye, that indicate the boundary and contour of the defected lattices.

the pseudospin qubits. To erase the information of two nonlinear-optic processes, pseudospin up and down states are coherently recombined at a two-dimensional grating coupler (Fig.1f). The grating diffracts entangled photons out-of-plane into free-space mode, enabling an arbitrary analysis of topological entanglement by mapping pseudospin to polarization states.

Figures 3c,d show experimental results of two-photon and four-photon quantum interference in the topological quantum emitters. The observations of double frequency interference fringe in Fig.3c and quadruple frequency interference fringe in Fig.3d, respectively, confirm the generation of two-photon pseudospin entanglement of $(|\uparrow\uparrow\rangle\,|vac\rangle + |vac\rangle\,|\downarrow\downarrow\rangle)/\sqrt{2}$ and four-photon pseudospin entanglement of $(|\uparrow\uparrow\uparrow\uparrow\rangle\,|vac\rangle + |vac\rangle\,|\downarrow\downarrow\downarrow\downarrow\rangle)/\sqrt{2}$ (photon number entangled states) in the topological edge modes, where $|vac\rangle$ is the vacuum state. Topological single-photon classical interference is shown in Fig.3b for comparison. For bulk modes, classical interference and quantum interference however fade away. Note that degenerated and non-degenerated spontaneous FWM processes were adopted for different measurements, and pseudo-photon-number-resolving measurement was applied in the generation of topological four-photon entanglement (see Sec.2 and Sec.3).

Figures 3e-h and Figure 4 present our main results. We generated a range of different topological quantum states, including the separated topological pseudospin up state $|\uparrow\uparrow\rangle$, pseudospin down state $|\downarrow\downarrow\rangle$, and the topological EPR entangled state of $(|\uparrow\uparrow\rangle + |\downarrow\downarrow\rangle)/\sqrt{2}$. To fully characterise these states, their density matrices were experimentally reconstructed by implementing over-complete quantum state tomography techniques[54]. All states are measured with a high state fidelity (F) and high purity (P), see their definitions in Fig.3 caption, that demonstrates the emergence of high quality topological quantum states. We remark that the topological EPR entangled state is reconstructed with a high fidelity of 0.968 ± 0.004, and high purity of 0.962 ± 0.008. We then verified the violation of a Clauser-Horne-Shimony-Holt (CHSH)-Bell type inequality[55]. We obtained the Bell value of 2.627 ± 0.027, which violates the local hidden variables model by 23.2 *s.d.*, conforming the presence of topological entanglement. As a comparison, bulk states were reconstructed with a low level of entanglement (see Fig. 3h). Moreover, Fig.S10 shows experimental results of one-dimensional and two-dimensional topological trivial quantum emitters, including measured field distributions and density matrices, which confirm the absence of entanglement due to fabrication disorders. It indicates that entanglement in the topological nontrivial edge modes is well protected against fabrication disorders, however it cannot be protected in trivial emitters.

Figure 4 reports experimental observations of topologically protected EPR entanglement in an imperfect emitter that is embedded with four different types of artificial structure defects. We devised the imperfect emitter by simultaneously adding and removing a single ring and a unit cell in the ring lattice structure (see Fig.4a). As Fig.4b shown, in the presence of strong structure defects, two topological edge states emerged explicitly in experiment (see simulation results in Fig.S3). Significantly, such robustness of topological phase results in the protection of quantum entanglement emitters against artificial structure defects. This is successfully confirmed by tomographic measurement of the topological EPR entangled state with a high state fidelity of 0.951 ± 0.010 and high purity of 0.910 ± 0.019,

Topological quantum states	Fidelity (F)	Purity (P)
❶ $\|\uparrow\uparrow\rangle$ [edge]	0.986 ± 0.004	0.981 ± 0.008
❷ $\|\downarrow\downarrow\rangle$ [edge]	0.987 ± 0.003	0.995 ± 0.006
❸ $(\|\uparrow\uparrow\rangle + \|\downarrow\downarrow\rangle)/\sqrt{2}$ [edge]	0.968 ± 0.004	0.962 ± 0.008
❹ $(\|\uparrow\uparrow\rangle + \|\downarrow\downarrow\rangle)/\sqrt{2}$ [bulk]	0.568 ± 0.016	0.572 ± 0.016
❺ $(\|\uparrow\uparrow\rangle + \|\downarrow\downarrow\rangle)/\sqrt{2}$ [edge,defect]	0.951 ± 0.010	0.910 ± 0.019
❻ $(\|\uparrow\uparrow\rangle + \|\downarrow\downarrow\rangle)/\sqrt{2}$ [bulk,defect]	0.351 ± 0.027	0.477 ± 0.016
❼ $(\|\uparrow\uparrow\rangle + \|\downarrow\downarrow\rangle)/\sqrt{2}$ [2D trivial]	0.361 ± 0.018	0.797 ± 0.023
❽ $(\|\uparrow\uparrow\rangle + \|\downarrow\downarrow\rangle)/\sqrt{2}$ [1D trivial]	0.457 ± 0.012	0.704 ± 0.019

Table 1 Summary of measured topological pseudospin quantum states. ❶ – ❹ states were generated in topological pseudospin edge modes or bulk modes in the Fig.1b device with no defects. ❺ and ❻ states were generated in the Fig.4a topological quantum device with artificial defects. ❼ and ❽ states were emerged in the trivial devices in Fig.S10. The value of F denotes quantum state fidelity, and P denotes state purity. All error bars (± 1 *s.d.*) are estimated from photon Poissonian statistics.

see Fig.4c, which are nearly identical to the measured results of the perfect emitter (Fig.3g). We thus demonstrate that genuine quantum entanglement is protected in topological quantum emitters with artificial defects. Entanglement however cannot be preserved any more in the bulk modes of the same device, see Fig.4d. Topological quantum devices also preserve robustness to more complex artificial defects, see an example in Fig.4e.

We have experimentally demonstrated the emission of topological quantum entanglement in the photonic anomalous Floquet topological insulators on silicon chips, without any needs of magnetic, cryogenic and vacuum operation of the device. The topological EPR entangled states have been experimentally verified by tomographical measurement and the violation of Bell inequality. Note the detection and locality loopholes were not closed in our measurement. We also note that our device does not break the time-reversal symmetry which may not possess resilience against some fabrication imperfections[43–46], such as the waveguide sidewall roughness that can cause back-reflection in the emitter (though backscattering does not lead to degradations of state fidelity and purity). This remains a general open question of all time-reversal invariant photonic insulators[15–17]. We rather focused on the demonstration of topologically-protected quantum entanglement emitters against artificially induced structure defects, which is directly confirmed by the preservation of measured state fidelity and purity for the topological nontrivial and trivial quantum emitters, see the summary in Table 1.

The benchmarking of topologically protected entanglement emitters can promote the investigations of other topological quantum photonic sources, circuits and devices[15–17,40–42], as well as matter-based topological quantum technologies in atomic, solid-state, and superconducting systems in which true interacting and topological quantum matter can be engineered[3]. Robust quantum topological devices may ultimately find applications in noisy intermediate-scale quantum information processing, simulation of quantum topological physics, and fault-tolerant quantum computing[33–36].

Note added – when our manuscript was in preparation, we became aware of an independent experiment[56]. Energy-time entanglement was generated in an anomalous quantum Hall photonic topological insulator together with bulk-optical and fiber-optical components, and topological robustness of the source was verified by numerical simulations. In our work, we demonstrated fully-integrated and plug-and-playable topological entanglement emitters, that generate topological EPR entangled states and topological multiphoton entangled states, and we experimentally verified the topological protection of EPR entangled states against artificial structure defects inside the emitters.

References

1. M. A. Nielsen & I. L. Chuang. *Quantum Computation and Quantum Information: 10th Anniversary Edition* (Cambridge University Press, 2010).
2. R. Horodecki, P. Horodecki, M. Horodecki & K. Horodecki. Quantum entanglement. *Rev. Mod. Phys.* **81,** 865–942 (2009).
3. M. Z. Hasan & C. L. Kane. Colloquium: Topological insulators. *Rev. Mod. Phys.* **82,** 3045–3067 (2010).
4. A. Einstein, B. Podolsky & N. Rosen. Can quantum-mechanical description of physical reality be considered complete? *Phys. Rev.* **47,** 777–780 (1935).
5. X.-L. Wang *et al.* 18-qubit entanglement with six photons' three degrees of freedom. *Phys. Rev. Lett.* **120,** 260502 (2018).
6. A. Omran *et al.* Generation and manipulation of Schrödinger cat states in Rydberg atom arrays. *Science* **365,** 570–574 (2019).
7. C. Song *et al.* Generation of multicomponent atomic Schrödinger cat states of up to 20 qubits. *Science* **365,** 574–577 (2019).
8. F. Arute *et al.* Quantum supremacy using a programmable superconducting processor. *Nature* **574,** 505–510 (2019).
9. H.-S. Zhong *et al.* Quantum computational advantage using photons. *Science* **370,** 1460–1463 (2020).
10. R. P. Feynman. Simulating physics with computers. *Int. J. Theor. Phys.* **21,** 467–488 (1982).
11. K. V. Klitzing, G. Dorda & M. Pepper. New method for high-accuracy determination of the fine-structure constant based on quantized Hall resistance. *Phys. Rev. Lett.* **45,** 494–497 (1980).
12. F. D. M. Haldane & S. Raghu. Possible realization of directional optical waveguides in photonic crystals with broken rime-reversal symmetry. *Phys. Rev. Lett.* **100,** 013904 (2008).
13. G. Jotzu *et al.* Experimental realization of the topological Haldane model with ultracold fermions. *Nature* **515,** 237–240 (2014).
14. Y. Poo, R.-X. Wu, Z. Lin, Y. Yang & C. T. Chan. Experimental realization of self-guiding unidirectional electromagnetic edge states. *Phys. Rev. Lett.* **106,** 093903 (2011).
15. L. Lu, J. D. Joannopoulos & M. Soljačić. Topological photonics. *Nature Photonics* **8,** 821–829 (2014).
16. T. Ozawa *et al.* Topological photonics. *Rev. Mod. Phys.* **91,** 015006 (2019).
17. A. B. Khanikaev & G. Shvets. Two-dimensional topological photonics. *Nat. Photon.* **11,** 763–773 (2017).
18. Z. Wang, Y. Chong, J. D. Joannopoulos & M. Soljačić. Observation of unidirectional backscattering-immune topological electromagnetic states. *Nature* **461,** 772–775 (2009).
19. M. Hafezi, E. A. Demler, M. D. Lukin & J. M. Taylor. Robust optical delay lines with topological protection. *Nat. Phys.* **7,** 907–912 (2011).
20. M. Hafezi, S. Mittal, J. Fan, A. Migdall & J. M. Taylor. Imaging topological edge states in silicon photonics. *Nat. Photon.* **7,** 1001–1005 (2013).
21. J.-W. Dong, X.-D. Chen, H. Zhu, Y. Wang & X. Zhang. Valley photonic crystals for control of spin and topology. *Nat. Mater.* **16,** 298–302 (2017).
22. S. Kruk *et al.* Nonlinear light generation in topological nanostructures. *Nat. Nanotechnol.* **14,** 126–130 (2019).
23. M. A. Bandres *et al.* Topological insulator laser: experiments. *Science* **359** (2018).
24. M. C. Rechtsman *et al.* Topological protection of photonic path entanglement. *Optica* **3,** 925–930 (2016).
25. Y. Wang *et al.* Topological protection of two-photon quantum correlation on a photonic chip. *Optica* **6,** 955–960 (2019).

26. K. Tschernig *et al.* Topological protection versus degree of entanglement of two-photon light in photonic topological insulators. *Nat. Commun.* **12,** 1974 (2021).
27. J.-L. Tambasco *et al.* Quantum interference of topological states of light. *Sci. Adv.* **4,** eaat3187 (2018).
28. Y. Chen *et al.* Topologically protected valley-dependent quantum photonic circuits. *Phys. Rev. Lett.* **126,** 230503 (2021).
29. S. Barik *et al.* A topological quantum optics interface. *Science* **359,** 666–668 (2018).
30. S. Mittal, E. A. Goldschmidt & M. Hafezi. A topological source of quantum light. *Nature* **561,** 502–506 (2018).
31. A. Blanco-Redondo, B. Bell, D. Oren, B. J. Eggleton & M. Segev. Topological protection of biphoton states. *Science* **362,** 568–571 (2018).
32. M. Wang *et al.* Topologically protected entangled photonic states. *Nanophotonics* **8,** 1327–1335 (2019).
33. J. Wang, F. Sciarrino, A. Laing & M. G. Thompson. Integrated photonic quantum technologies. *Nat. Photon.* **14,** 273–284 (2020).
34. F. Flamini, N. Spagnolo & F. Sciarrino. Photonic quantum information processing: a review. *Reports on Progress in Physics* **82,** 016001 (2018).
35. A. W. Elshaari, W. Pernice, K. Srinivasan, O. Benson & V. Zwiller. Hybrid integrated quantum photonic circuits. *Nat. Photon.* **14,** 285–298 (2020).
36. J.-H. Kim, S. Aghaeimeibodi, J. Carolan, D. Englund & E. Waks. Hybrid integration methods for on-chip quantum photonics. *Optica* **7,** 291–308 (2020).
37. D. Llewellyn *et al.* Chip-to-chip quantum teleportation and multi-photon entanglement in silicon. *Nat. Phys.* **16,** 148–153 (2020).
38. J. Wang *et al.* Experimental quantum Hamiltonian learning. *Nat. Phys.* **13,** 551–555 (2017).
39. J. Wang *et al.* Multidimensional quantum entanglement with large-scale integrated optics. *Science* **360,** 285–291 (2018).
40. M. Segev & M. A. Bandres. Topological photonics: Where do we go from here? *Nanophotonics* **10,** 425–434 (2021).
41. Z. Chen & M. Segev. Highlighting photonics: looking into the next decade. *eLight* **1,** 2 (2021).
42. A. Blanco-Redondo. Topological nanophotonics: toward robust quantum circuits. *Proceedings of the IEEE* **108,** 837–849 (2020).
43. G. Q. Liang & Y. D. Chong. Optical resonator analog of a two-dimensional topological insulator. *Phys. Rev. Lett.* **110,** 203904 (2013).
44. M. Pasek & Y. D. Chong. Network models of photonic Floquet topological insulators. *Phys. Rev. B* **89,** 075113 (2014).
45. F. Gao *et al.* Probing topological protection using a designer surface plasmon structure. *Nat. Commun.* **7,** 11619 (2016).
46. S. Afzal, T. J. Zimmerling, Y. Ren, D. Perron & V. Van. Realization of anomalous Floquet insulators in strongly coupled nanophotonic lattices. *Phys. Rev. Lett.* **124,** 253601 (2020).
47. M. S. Rudner, N. H. Lindner, E. Berg & M. Levin. Anomalous edge states and the bulk-edge correspondence for periodically driven two-dimensional systems. *Phys. Rev. X* **3,** 031005 (3 2013).
48. L. J. Maczewsky, J. M. Zeuner, S. Nolte & A. Szameit. Observation of photonic anomalous Floquet topological insulators. *Nat. Commun.* **8,** 13756 (2017).
49. S. Mukherjee *et al.* Experimental observation of anomalous topological edge modes in a slowly driven photonic lattice. *Nat. Commun.* **8,** 13918 (2017).
50. L. J. Maczewsky *et al.* Fermionic time-reversal symmetry in a photonic topological insulator. *Nat. Mater.* **19,** 855–860 (2020).
51. Y. Ao, X. Hu, C. Li, Y. You & Q. Gong. Topological properties of coupled resonator array based on accurate band structure. *Phys. Rev. Mater.* **2,** 105201 (2018).
52. S. Afzal & V. Van. Topological phases and the bulk-edge correspondence in 2D photonic microring resonator lattices. *Opt. Express* **26,** 14567–14577 (2018).
53. A. Dutt *et al.* A single photonic cavity with two independent physical synthetic dimensions. *Science* **367,** 59–64 (2020).
54. D. F. V. James, P. G. Kwiat, W. J. Munro & A. G. White. Measurement of qubits. *Phys. Rev. A* **64,** 052312 (5 2001).
55. J. F. Clauser, M. A. Horne, A. Shimony & R. A. Holt. Proposed experiment to test local hidden-variable theories. *Phys. Rev. Lett.* **23,** 880–884 (1969).
56. S. Mittal, V. V. Orre, E. A. Goldschmidt & M. Hafezi. Tunable quantum interference using a topological source of indistinguishable photon pairs. *Nat. Photon.* (2021).

Acknowledgements We acknowledge support from the National Key R&D Program of China (nos 2019YFA0308702, 2018YFB1107205, 2018YFB2200403, 2018YFA0704404, 2016YFA0301302), the Natural Science Foundation of China (nos 61975001, 61590933, 61904196, 61675007, 61775003, 11734001, 91950204, 11527901), Beijing Natural Science Foundation (Z190005), Beijing Municipal Science & Technology Commission (Z191100007219001) and Key R&D Program of Guangdong Province (2018B030329001). L. Y. also acknowledges support from Natural Science Foundation of Shanghai (19ZR1475700) and the Program for Professor of Special Appointment (Eastern Scholar) at Shanghai Institutions of Higher Learning.

Authors contributions J.W. convinced the project. T.D., Y.A., J.B., J.M., and Y.C. contributed equally to this work. T.D., J.B., and Z.F. implemented the experiment. J.M., Y.C., B.T., Y.Y., and Z.L. fabricated the device. T.D., Y.A., J.B., and X.C. designed the devices. Y.A. and Y.Y. provided the theory and simulations. T.D., Y.A., Z.F., C.Z., L.Y., F.G., and X.L. performed the theoretical analysis. M.G.T., J.L.O., Y.L., X.H., Q.G., and J.W. managed the project. T.D., Y.A., and J.W. write the manuscript. All authors discussed the results and contributed to the manuscript.

Competing interests: All authors declare no competing final interests.

Supplementary Files

This is a list of supplementary files associated with this preprint. Click to download.

- SupplementaryinformationTopologicallyProtectedQuantumEntanglementEmitters.pdf
- MovieS1.mp4
- MovieS2.mp4
- MovieS3.mp4